Eur. Phys. J. B **14**, 459–471 (2000)

THE EUROPEAN PHYSICAL JOURNAL B

EDP Sciences
© Società Italiana di Fisica
Springer-Verlag 2000

Peculiarities in low temperature properties of doped manganites $A_{1-x}B_xMnO_3$

M.O. Dzero[1,a], L.P. Gor'kov[1,2], and V.Z. Kresin[3]

[1] National High Magnetic Field Laboratory, Florida State University, Tallahassee, FL 32310, USA
[2] L.D. Landau Institute for Theoretical Physics, Russian Academy of Sciences, 117334 Moscow, Russia
[3] Lawrence Berkeley Laboratory, University of California, Berkeley, CA 94720, USA

Received 22 September 1999

Abstract. The phase diagram and low temperature properties of the doped manganites $\mathrm{A}_{1-x}\mathrm{B}_x\mathrm{MnO}_3$ are discussed for the concentrations $x \leq 0.4$. The transition from insulating antiferromagnetic to metallic ferromagnetic state at $x_{\mathrm{cr}} \simeq 0.16$ is treated by means of percolation theory. The unifying description of insulating and metallic states is presented. The undoped manganite is a band insulator consisting of ferromagnetic layers, which are coupled antiferromagnetically along the c direction with a low Néel temperature. The metallic phase can be described by the two-band Fermi liquid picture. The behavior of conductivity, spin wave excitations, etc. is analyzed and the comparison with experimental data is carried out.

PACS. 72.15.Gd Galvanomagnetic and other magnetotransport effects – 75.30.Ds Spin waves

1 Introduction

Interest in utilizing the "colossal magnetoresistance" (CMR) effect has resulted in enormous literature, which spans properties of manganites at numerous compositions, ceramic and crystals, crystalline films on different substrates, stoichiometric and not (for extensive review see [1,2]). Nevertheless, until recently, it was somewhat difficult to establish systematic trends which govern the physical properties of these materials (especially their low temperature behavior), to access peculiarities pertinent to the ground state and its dependence on composition.

As for the overall behavior, especially for the high temperature properties, which are responsible for the CMR phenomena itself, the consensus is that the Zener's double exchange (DE) mechanism [3–5] together with the Jahn-Teller (JT) effect for Mn^{3+} as suggested in [6,7] produce the basis for their understanding. High temperature lattice deformations localize carriers by a formation of the JT or local polarons [6,8]. With temperature decrease, DE mechanism delocalizes carriers and result in simultaneous onset of metallic conductivity and half-metallic ferromagnetic state. The physical picture, is by all means correct, but the method, introduced in [6], is not sufficient for understanding delicate qualitative features, especially at the low temperatures.

As an important issue, we have to mention, is the evolution of ground state for the doped manganites from the insulating antiferromagnetic state of LaMnO_3 to the pronounced metallic ferromagnetic one in $\mathrm{La}_{1-x}\mathrm{Sr}_x\mathrm{MnO}_3$ at $x \sim 0.3$.

It has been demonstrated first in our short paper [9] that both the half-metallic state at finite concentrations and the insulating state of the parent LaMnO_3 can be brought together by making use of a simple band model. Parent LaMnO_3 is considered in that scheme as a band insulator. As for the doping process, it has been shown in [9], that it leads to the percolative scenario, producing the well defined threshold concentration $x_{\mathrm{cr}} \sim 0.16-0.17$ for the onset of low-temperature metallic conductivity.

In the presentation below we describe in more details and further elaborate the theory, proposed by Gor'kov and Kresin, keeping in mind both some future applications and analysis of available experimental data at $x \leq 0.4$ is also provided. It is shown that the two bands theory agrees reasonably well with the results of recent experiments, demonstrating applicability of the Fermi liquid approach to the metallic manganites. The scheme serves as a theory unifying rather rich low temperature properties of manganites and is capable of some predictions regarding the evolution of physical parameters, the shape of the Fermi surface etc. with concentration. The experimental data show also the consistency with our results in the metallic concentration range and trace remaining percolation features.

The paper is written as follows. In Section 2 the main features are identified and accounted in Hamiltonian. Section 3 contains the energy spectrum and its dependence

---

[a] e-mail: `dzero@magnet.fsu.edu`

on a spin ordering or JT-deformations. Properties of a stoichiometric compound $\mathrm{LaMnO_3}$, treated as a band insulator, are considered in Section 4. Growth of the percolative regime for the phase separation and the critical composition for onset of metallic conduction are discussed in Section 5. Section 6 contains a summary of major metallic properties calculated in the framework of the two band model, while in Section 7 a comparison with available experimental data is discussed. Section 8 contains brief summary and conclusions.

2 Model and Hamiltonian

We just start with, a somewhat oversimplified (the so-called "pseudocubic") crystalline structure for manganites. As it is well-known [1,2], in that approximation the unit cell, say, for $\mathrm{LaMnO_3}$, may be taken as a cube, with the lattice constant $a_0 \simeq 3.9$ Å. Rare-earth or alkaline ions are placed at the center, while the manganese ions occupy the corner sites. $\mathrm{Mn^{3+}}$-sites are caged into the oxygen octahedra, which share the $\mathrm{O^{2-}}$ ions along the Mn-O-Mn bond (another view would be that each $\mathrm{La^{3+}}$-ion is cooped up in the midst of twelve $\mathrm{O^{2-}}$ ions). The ideal structure is then modified for real materials, $\mathrm{AMnO_3}$, due to a mismatch in the ionic radii. The latter is commonly characterized by the tolerance factor, t (see *e.g.* in [1]):

$$t = \frac{1}{\sqrt{2}}\frac{R_{\mathrm{A}} + R_{\mathrm{O}}}{R_{\mathrm{Mn}} + R_{\mathrm{O}}} \cdot \tag{1}$$

The effect of $t \neq 1$ is that the oxygen octahedra become periodically tilted, and the unit cell may then be comprised of a few "pseudocubic" cells. It is shown below that deviations from the "pseudocubic" structure, *i.e.* deviations in the angle, α, of the Mn-O-Mn bond from 180° are not of much importance for the "average" electronic structure. However, we will see later that *local* fluctuations in the tolerance factor (1) may play rather significant role for the conducting properties of the "doped" manganites $\mathrm{A_{1-x}B_xMnO_3}$.

Let us outline our base model which is then applied for the interpretation of manganites properties. Since the manganese d-shell has reasonably small orbitals, the model exploits the tight binding approximation.

As it is well known, the $\mathrm{Mn^{3+}}$ ion has four d-electrons. The d-shell in the cubic environment is split into the triple (t_{2g}) and double (e_{2g}) degenerate terms. The t_{2g}-level is fully occupied by three electrons considered as a local spin $S = 3/2$, in accordance with the Hund's rule. The e_{2g}-term in manganites may be empty ($\mathrm{Mn^{4+}}$) or single occupied ($\mathrm{Mn^{3+}}$). If there is one electron on the e_{2g}-level, the direction of its spin is governed by the same intra-atomic Hund's interaction:

$$\hat{H}_{\mathrm{H}} = -J_{\mathrm{H}}\boldsymbol{\sigma} \cdot \mathbf{S}_i, \tag{2}$$

($\boldsymbol{\sigma}$– the Pauli matrix for the e_{2g}-electron). The Hund's coupling $J_{\mathrm{H}} > 0$ is rather large ($J_{\mathrm{H}}S \sim 1 \div 1.5$ eV). Therefore spins of e_{2g} and t_{2g} electrons are ferromagnetically aligned locally.

The two major assumptions are: 1. the splitting between the t_{2g}- and e_{2g}-levels is large enough, so that only e_{2g} electrons may participate in conductivity; 2. the e_{2g}-levels are well above the top of the filled up oxygen band (on a scale of a few eV). The band-structure calculations do not always support the last assertion (see *e.g.* [10]). On the other hand, extensive optical studies agree well with the second assumption, see *e.g.* [11].

Hoping process of one electron from a site i to its nearest neighbor $i + \delta$ in the tight-binding approximation has to be modified to account for the double degeneracy of the e_{2g}-level on each site. In the hopping Hamiltonian, hence:

$$\hat{H}_t = \sum_{i,\delta} \hat{t}_{i,i+\delta}, \tag{3}$$

$\hat{t}_{i,i+\delta}$ becomes a two-by-two matrix. Its explicit form depends on choice of the basis for the e_{2g}-representation.

The e_{2g}-degeneracy of the $\mathrm{Mn^{3+}}$ site would locally result in the Jahn-Teller (JT) instability with respect to spontaneous lattice distortions. Two active modes for deformation of the surrounding oxygen octahedron are usually denoted in literature as Q_2 and Q_3 (see [12] and review [13]), and form the two-dimensional basis of the octahedron deformations. In the invariant form the JT part of the electron-lattice interaction may be written as:

$$H_{\mathrm{JT}} = g\ \hat{\boldsymbol{\tau}}_i \cdot \mathbf{Q}_i, \tag{4}$$

where $\hat{\boldsymbol{\tau}}$ is called the "pseudospin" matrix (see [13]).

In what follows we use the normalized complex basis [9,14] for the two-dimensional representation e_{2g}:

$$\psi_1 \propto z^2 + \epsilon x^2 + \epsilon^2 y^2;\ \psi_2 \equiv \psi_1^*, \tag{5}$$

where $\epsilon = \exp(2\pi \mathrm{i}/3)$. Another basis, which is often used in literature, for example [13,15], is given by the real functions:

$$\varphi_1 \propto d_{z^2} \equiv 3z^2 - (x^2 + y^2);\ \varphi_2 \propto d_{x^2-y^2} \equiv x^2 - y^2. \tag{5'}$$

Connection between these two is:

$$\psi_1 = (\varphi_1 + \mathrm{i}\varphi_2)/\sqrt{2};\ \psi_2 \equiv \psi_1^*. \tag{5''}$$

The given basis (5) makes it possible to present (4) in the convenient form:

$$-\frac{g}{2}Q_0 \begin{pmatrix} 0 & \exp(\mathrm{i}\theta) \\ \exp(-\mathrm{i}\theta) & 0 \end{pmatrix} \tag{6}$$

where in the standard notations [12,13,15]:

$$Q_2 = Q_0 \sin\theta\ ;\ Q_3 = Q_0 \cos\theta \tag{7}$$

with Q_0 being the magnitude of the JT-distortions. The angle, θ, specifies the shape of the distorted octahedron. Thus, the angles $\theta = 0, \pm 2\pi/3$ correspond to elongation of the octahedron along the z, x and y-axes, respectively.

The JT-term (4) is linear in Q, while the elastic energy is quadratic in Q. Therefore if one electron is placed on the JT-level, the total site energy always decreases with non-zero lattice deformations. Strictly speaking, deformations, Q_i, on the two adjacent manganese sites are not independent because the two sites share one oxygen along the Mn-O-Mn bond; in what follows only cooperative JT distortions will be considered.

According to review [12] (see also [13]) we are dealing with two normal modes Q_2 and Q_3, where:

$$\begin{aligned} Q_2 &= \frac{1}{\sqrt{2}}(x_1 - x_4 + y_5 - y_2), \\ Q_3 &= \frac{1}{\sqrt{6}}(2z_2 - 2z_6 - x_1 - x_4 - y_2 + y_5). \end{aligned} \tag{8}$$

Onset of the cooperative JT distortions means the onset of a non-cubic structural order ("ferrodistorsive" deformations, if the wave vector of the structure, $\mathbf{q} = 0$, "antiferrodistorsive" ones, if $\mathbf{q} \neq 0$ [12,16]). To account for fluctuations or changes in the phonon spectrum, the displacements in (8) must be expressed in terms of the normal modes for the crystal vibrations.

With the above remark regarding the JT-distortion, one may now bring all the contributions (2,3,4) together:

$$H = \sum_i \left(\sum_\delta \hat{t}_{i,i+\delta} - J_{\mathrm{H}} \boldsymbol{\sigma} \cdot \mathbf{S}_i + g \hat{\boldsymbol{\tau}}_i \cdot \mathbf{Q}_i + J_{\mathrm{el}} \mathbf{Q}_i^2 \right) \tag{9}$$

(the last term added into (9) is responsible for the "elastic" energy of the JT mode). The Hamiltonian of exactly the form (9) has been considered by Millis *et al.* [6,7]. As it was mentioned above, the important physical observation made in [6,7] was that with the temperature increase disorder produced by thermally excited JT degrees of freedom tends to localize the charge carriers. Though the idea by all means is qualitatively correct, the approach, used in [6], is a selfconsistent interpolative scheme which is not appropriate for understanding low temperature properties of manganites, *i.e.* the symmetry of the ground state and its variation with composition. The latter issues are addressed below mainly in terms of the band approach.

3 Band spectrum

Let us consider first the band spectrum of the Hamiltonian (3,4) (the Hund's term and JT term being temporary omitted). The matrix $\hat{t}$ in (3) on the basis (5) has the form:

$$\begin{pmatrix} \Sigma_{11} & \Sigma_{12} \\ \Sigma_{21} & \Sigma_{22} \end{pmatrix}, \tag{10}$$

where

$$\begin{aligned} \Sigma_{11} &= \Sigma_{22} = \Sigma_0 = (A+B)[\cos(k_x a) + \cos(k_y a) + \cos(k_z a)], \\ \Sigma_{12} &= \Sigma_{21}^* = (A-B)[\cos(k_z a) + \epsilon \cos(k_x a) + \epsilon^2 \cos(k_y a)]. \end{aligned} \tag{11}$$

A and B in (11) are two overlap integrals:

$$\begin{aligned} A &\propto \overline{\varphi_1(z; x, y)\varphi_1(z+a; x, y)}, \\ B &\propto \overline{\varphi_2(z; x, y)\varphi_2(z+a; x, y)}, \end{aligned} \tag{12}$$

where the bar $\overline{(...)}$ means the matrix elements for the interaction potential on the two Wannier functions, $\varphi_{1,2}$, of the neighboring atoms (in the tight binding approximation $A = -|A| < 0$). Simple geometric considerations for the d-shell show that $|B| < |A|(|B| \simeq \frac{1}{16}|A|$, according to [17,18]). The cubic spectrum consists of the two branches:

$$\begin{aligned} \varepsilon_{1,2}(\mathbf{p}) = &-(|A| + |B|)(c_x + c_y + c_z) \\ &\pm (|A| - |B|)\sqrt{c_x^2 + c_y^2 + c_z^2 - c_x c_y - c_y c_z - c_z c_x} \end{aligned} \tag{13}$$

(we introduced the notations $c_i = \cos(k_i a), i = x, y, z$).

If a homogeneous "ferroelastic" JT-distortion is imposed on the lattice, the spectrum may be obtained by adding $-\frac{gQ_0}{2}\exp(i\theta)$ term to Σ_{12} in (10). For some future applications we provide here the spectrum for the limiting case $|gQ_0| \gg |A|$:

$$\begin{aligned} \widetilde{\varepsilon}_{1,2}(\mathbf{p}) = &\pm \left| \frac{gQ_0}{2} \right| + (A+B)(c_x + c_y + c_z) \\ &\pm (A-B) \left\{ (c_z - \frac{1}{2}(c_x + c_y)) \cos(\theta) + \frac{\sqrt{3}}{2}(c_y - c_x) \sin(\theta) \right\}. \end{aligned} \tag{14}$$

This expression is interesting: at the choice $\sin(\theta) = 0$ the low-lying electronic branch would become strongly anisotropic ($|B| \ll |A|$):

$$\widetilde{\varepsilon_2}(\mathbf{p}) = -\left| \frac{gQ_0}{2} \right| - 2Bc_z + \frac{3}{2}A(c_x + c_y). \tag{14'}$$

Returning to the full electronic Hamiltonian, let us recall that the Hund's term (2) is the largest one: we assume below $J_{\mathrm{H}} \gg |A|, gQ$. Therefore in all cases the electronic spectrum is shifted up or down by the energy $\pm J_{\mathrm{H}} S$, depending on the e_{2g} and t_{2g} *mutual* spin direction. At the ferromagnetic alignment of the all local and itinerant spins *each of* the two branches of equation (13) merely splits into two by adding the $\pm J_{\mathrm{H}} \langle S \rangle$ energy term. For an antiferromagnetic (AF) ground state one needs to calculate the energy spectrum again. It is done below for the important case of two "canted" antiferromagnetic sublattices when a ferromagnetic spin component $\mathbf{M}_i$ coexists with the staggered magnetization, $\mathbf{S}_i = (-1)^i \mathbf{S}_i$. We assume that antiferromagnetic ordering with the structure vector $\mathbf{q}$, runs along the c-axis, $\mathbf{q} = \frac{\pi}{a}(0, 0, 1)$. Such an AF-structure is often dubbed as the A-phase.

We will perform our calculations treating local $\mathbf{M}_i$ and $\mathbf{S}_i$ as the classical vectors: $(\mathbf{M}_i + \mathbf{S}_i)^2 = \mathbf{S}^2; |\mathbf{S}| = 3/2$. The e_{2g}-electron wave function in the momentum representation acquires the form:

$$\Psi_{\mathbf{p}} \equiv \left\{ \begin{array}{c} \alpha_{\mathbf{p}\sigma}\psi_1 \\ \beta_{\mathbf{p}\sigma}\psi_2 \end{array} \right\} => \left\{ \begin{array}{c} \alpha_{\mathbf{p}\sigma} \\ \beta_{\mathbf{p}\sigma} \end{array} \right\}, \tag{15}$$

where now $\alpha_{\mathbf{p}\sigma}, \beta_{\mathbf{p}\sigma}$ have a nontrivial spin-index dependence. Let $\mathbf{S}(\mathbf{q})$, the staggered magnetization component, be directed along the z-direction, while $\mathbf{M}$ is parallel to the x-axis (in the spin space). In the calculations below we suppose $\mathbf{q}$ is along c-axis. The Brillouin zone is reduced along the c-direction, in accordance with a choice of $\mathbf{q}$-vector. The energy spectrum is determined by the following equations:

$$\hat{E}\psi_{\mathbf{p}\sigma} = (\hat{t}(\mathbf{p}) - J_{\mathrm{H}}\hat{\sigma}_x M)\psi_{\mathbf{p}\sigma} - J_{\mathrm{H}}\hat{\sigma}_z S\psi_{\mathbf{p}+\mathbf{q}\sigma},$$
$$\hat{E}\psi_{\mathbf{p}+\mathbf{q}\sigma} = (\hat{t}(\mathbf{p}+\mathbf{Q}) - J_{\mathrm{H}}\hat{\sigma}_x M)\psi_{\mathbf{p}+\mathbf{q}\sigma} - J_{\mathrm{H}}\hat{\sigma}_z S\psi_{\mathbf{p}\sigma}.$$

Multiplying each equation by $\hat{\sigma}_z$ and eliminating $\psi_{\mathbf{p}+\mathbf{q}\sigma}$, one arrives to the following two-by-two matrix equation:

$$\left[\hat{E} - \hat{t}_{\mathbf{p}+\mathbf{q}} - J_{\mathrm{H}}\hat{\sigma}_x M\right]\left[\hat{E} - \hat{t}_{\mathbf{p}} + J_{\mathrm{H}}\hat{\sigma}_x M\right]\psi_{\mathbf{p}} = J_{\mathrm{H}}^2 S^2\psi_{\mathbf{p}}$$

or

$$\left[E^2 - 2\hat{t}_{p_x,p_y}E + 2J_{\mathrm{H}}\hat{\sigma}_x M\hat{t}_{p_z} + \hat{t}^2_{p_x,p_y} - \hat{t}^2_{p_z}\right]\psi_{\mathbf{p}} = J_{\mathrm{H}}^2 S^2\psi_{\mathbf{p}}, \tag{16}$$

where we have separated in the $\hat{t}$-matrix its dependence on the momenta parallel and perpendicular to the direction of the $\mathbf{q}$-vector:

$$\hat{t} = \hat{t}_{p_x,p_y} + \hat{t}_{p_z}$$

and also we have used that $\hat{t}_{p_z+q_z} \equiv -\hat{t}_{p_z}$. Equation (16) gives $E_0 = \pm J_{\mathrm{H}}S$ in the zeroth approximation, as expected. Taking $E = -J_{\mathrm{H}}S + \varepsilon$, we obtain:

$$\Big[\varepsilon^2 - 2J_{\mathrm{H}}S\varepsilon + 2\hat{t}_{p_{p_x,p_y}}(J_H S - \varepsilon)$$
$$+2J_{\mathrm{H}}\hat{\sigma}_x M\hat{t}_{p_z} + \hat{t}^2_{p_x,p_y} - \hat{t}^2_{p_z}\Big]\psi_{\mathbf{p}} = 0. \tag{16'}$$

For the next approximation ($\varepsilon \sim \hat{t}$) in (16'):

$$\hat{\varepsilon}\psi_{\mathbf{p}} = \left[\hat{t}_{p_x,p_y} + \hat{\sigma}_x\frac{M}{S}\hat{t}_{p_z}\right] \equiv \left[\hat{t}_{p_x,p_y} + \hat{\sigma}_x\cos(\theta/2)\hat{t}_{p_z}\right]\psi_{\mathbf{p}}, \tag{17}$$

i.e. one obtains the generalized Anderson-Hasegawa term for the motion along the c-axis. Equation (17) is the four-by-four matrix: two-by-two due to the orbital degeneracy and two-by-two due to the spin variables. After diagonalization over the spin variables, it provides the following tunneling matrix:

$$\hat{\varepsilon}^{(1)}_{\pm} = \hat{t}_{p_x,p_y} \pm \cos(\theta/2)\ \hat{t}_{p_z}. \tag{18}$$

To obtain the new spectrum one merely has to make a substitution in equation (13): $c_z \rightarrow \cos(\frac{\theta}{2})c_z$ (the number of energy branches is doubled because of reduction of the Brillouin zone at doubling the periodicity along the c-direction. If, in addition, there is a homogeneous JT deformation, all $\hat{t}_{p_x,p_y}$ and $\hat{t}_{p_z}$ must be changed in the same manner as it has been done above). In accordance with the DE-mechanism, any connection between adjacent ferromagnetic layer in the A-phase fully disappears in the approximation (18). To find further approximations, one has to take into account small terms of the order of $t^2/J_{\mathrm{H}} \ll t$. The analysis below produces the scale for t in (13): $|A| \sim 0.16$ eV, *i.e.* these terms should be reasonably small and may be neglected except for some more peculiar phenomena in doped manganites. Regarding the magnitude of the JT-component, equations (4, 7), it is suggested below that main physics to large extent depends on competition between the energy gained in the JT-distortions and kinetic (band) energy of electrons. Correspondingly, the JT-term is generally assumed to be of the same order as $|A|\ gQ_0 \sim |A|$, in our model.

4 Parent manganite as a band insulator

At low temperatures the stoichiometric ends of materials in series $\mathrm{A}_{1-x}\mathrm{B}_x\mathrm{MnO}_3$ are insulators. For the "right" end ($x = 1$) it causes no surprise: all manganese ions are Mn^{4+}, *i.e.* comprise of the localized t_{2g}-spins. The magnetic properties are then described by an effective Heisenberg Hamiltonian commonly attributed to the superexchange mechanisms along the Mn-O-Mn bonds (the Hamiltonian itself may be constructed by the so-called "Anderson-Goodenough-Kanamori rules" (see in [5,12, 17]). For the same approach to be applied for the "left" end ($x = 0$, LaMnO_3), one should similary treat the Mn^{3+} e_{2g}-shells as localized spin orbitals. All pertinent properties are often interpreted in terms of generalized microscopic Hubbard model (see *e.g.* [13,15]). The key feature of the Hubbard model is the assertion that for two electrons to be placed on the same site the energy cost is very high (the famous Hubbard "U" > 0 due to the on-site Coulomb repulsion!).

The Hubbard Hamiltonian approach has been challenged in [9]. First, there are experimental motivations for such challenge. For instance it was shown than in "doped" manganites, $\mathrm{La}_{1-x}\mathrm{Sr}_x\mathrm{MnO}_3$, at rather low concentrations, say, $x = 0.2$, the system displays excellent low T metallic behavior [19]. Meanwhile, the nominal number of e_{2g}-electrons per Mn site, $N = 1 - x < 1$, was changed only by one fifth in this study. From the theoretical side, it is of course clear that dealing with the strictly atomic d-orbitals would be a strong oversimplification. If a Mn ion is placed into the oxygen octahedron environment, the e_{2g}-terms are formed by the whole ligand, so that the "pure" d-functions become considerably hybridized with the surrounding oxygen states (*e.g.* see the discussion in [10,18]). Hence the electronic polarization would undoubtly reduce the magnitude of the "Hubbard"-like (on-site) interactions. Finally, for the JT-effect (which itself is nothing but another form of the Coulomb interaction) to come up there is no need to use the Mn^{3+} localized states picture as it will be seen from what is done below. The JT effect may persist even in the band model.

Therefore, in what follows, we adopt the band approach to describe the ground state of LaMnO_3. This approach rationalizes the major features of an insulating state in LaMnO_3 very well and merge into metallic state of "doped" manganites (see [20]).

Experimentally it is known [1] that $LaMnO_3$ transforms into the AF state below the Néel temperature, $T_N \simeq 140$ K. Its magnetic structure corresponds to the A-phase, *i.e.*, consists of ferromagnetically aligned layers which are coupled antiferromagntically along the one of main axes (that axis is chosen as c-axis below). As for the lattice, the cubic cell becomes compressed along the same direction because the oxygen octahedra exercise the collective JT ordering: the octahedra are elongated along x- or y-direction and are packed as it is shown schematically in Figure 1. Correspondingly, the periodicity is doubled in the (x, y) plane by the JT-distortions, and is also doubled by the A-phase magnetic superstructure along the z-axis. Simple considerations will show that calculating the band spectrum for such a superstructure and filling the bands at one electron per manganese site immediately lead to the band insulator ground state.

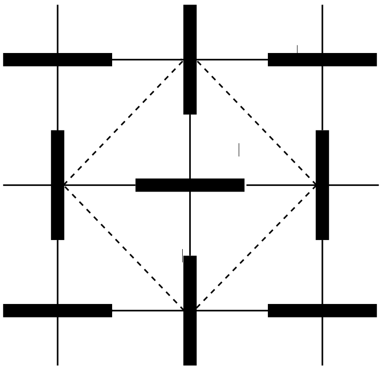

Fig. 1. In-plane staggered distortions inside the ferromagnetic layer. Solid segments represent the elongations of octahedra. The new unit cell is shown as the dashed square.

We preface these calculations with a brief discussion of the role of DE mechanism for a more simple model in which each "manganese" site has only one orbital for mobile electrons (in addition to localized spin $\mathbf{S}_i$, of course). Instead of (13), one has now the tight binding spectrum:

$$\varepsilon(\mathbf{p}) = t(\cos(p_x a) + \cos(p_y a) + \cos(p_z a)). \quad (19)$$

Imposing the Hund's term (2), $J_H \gg t$, the energy of an electron in the "half-metallic" (fully polarized) state, $\varepsilon_{hm}(\mathbf{p})$, is:

$$\varepsilon(\mathbf{p}) = -J_H S + \varepsilon(\mathbf{p}) \quad (19')$$

and the electronic contribution to the total energy:

$$E^F_{el} = \int \varepsilon_{hm}(\mathbf{p}) n_{\mathbf{p}} \frac{d^3p}{(2\pi\hbar)^3} \equiv -J_H S. \quad (20)$$

(per cubic unit cell).

Rederiving equation (16) in the simplified case described above for the A-phase, it is easy to find the electronic energy of the A-phase ($\mathbf{M} \simeq 0$ in (16)):

$$E^A_{el} = -\int \sqrt{(J_H S)^2 + t^2_{\mathbf{p}}} \frac{d^3p}{(2\pi\hbar)^3} \simeq -J_H S - \frac{t^2}{4\, J_H\, S}\,. \quad (20')$$

From (20) and (20') one may conclude first, that terms of the order of t^2/J_H in the electronic energy make the AF-state (the A-phase) energetically more favorable. That gain, being small, should be considered together with the superexchange contributions, if any. Moreover, both equations (20) and (20') were obtained for the "stoichiometric" case of one electron per Mn site. The DE mechanism in cooperation with large value of J_H makes all electrons have only one spin direction. Therefore, the bands in (20) and (20') are fully occupied. In *both* cases (ferromagnegnetic and antiferromagnetic states) one would obtain the insulating phase for that model.

Returning to the more realistic situation of the e_{2g}-level, the two bands, and the A-type antiferromagnetic order, it follows again from equation (18) that in the main approximation the problem reduces to constructing the ground state of a single ferromagnetic layer. Unlike the previous case, a "simple" ferromagnetic state would be metallic because of the two bands:

$$\varepsilon_{\pm}(\mathbf{p}) = -|A|(c_x + c_y) \pm |A|\sqrt{c_x^2 + c_y^2 - c_x c_y} \quad (13')$$

(since $|B| \ll |A|$ as was mentioned above, the B-part in (13) was neglected) and one electron per cell. The Brillouin zone will be only half-filled (all electrons are polarized). Superstructure imposed by the JT deformations, as shown in Figure 1, suggests that since the Brillouin zone is now reduced by a factor of two, the same number of electrons may fill up the reduced zone, producing an insulator at the appropriate energy spectrum. Experimentally, $LaMnO_3$ *is* an insulator and it is interesting to find the electronic band spectrum in the presence of the cooperative JT-distortions and then discuss the spectrum properties together with the experimental findings.

Before we proceed further, let us make one remark. As it is well known, two dimensional ferromagnetic state is never stable being destroyed by spin fluctuations. Stabilization of the A-phase comes up due to the small terms in energy, which are responsible for remnant interactions between layers. Our estimates below for $|A| \sim 0.16$ eV and $J_H S \sim 1.5$ eV would place the terms $\sim t^2/J_H$ on the scale of $\sim 100K$ which agrees well with the low value of the Néel temperature, $T_N \simeq 150$ K.

However, "superexchange" terms, $J\, \mathbf{S}_i \cdot \mathbf{S}_j$, with J, being on the same scale as $\sim t^2/J_H$, may also become important. Role of these interaction at the small "electron" doping (*i.e.* close to the $CaMnO_3$ end) has recently been discussed in terms of the band picture in [21].

To calculate the electronic spectrum of our model in the presence of the "antiferrodistorsive" JT collective deformations shown in Figure 1, let us note that the structure vector of the superlattice is $\mathbf{q} = \frac{\pi}{a}(1, 1, 0)$. The superstructure shows up in the JT-term (7) and depends on which of the two modes (Q_2, Q_3 or even their superposition) of equation (7) is chosen to correspond to the JT local deformations on each of the two sublattices. Experimentally, the arrangement in Figure 1 is close to the one in which octahedra are elongated along each x- or y-axis preserving the tetragonal symmetry in

$$\begin{vmatrix} \left[\varepsilon^2 - (gQ_0/2)^2 - \frac{5}{4}f_+^2 + \frac{3}{4}f_-^2\right] + \mathrm{i}\frac{\sqrt{3}}{2}f_+f_- & f_+^2 - \mathrm{i}\varepsilon\sqrt{3}f_- \\ f_+^2 + \mathrm{i}\varepsilon\sqrt{3}f_- & \left[\varepsilon^2 - (gQ_0/2)^2 - \frac{5}{4}f_+^2 + \frac{3}{4}f_-^2\right] - \mathrm{i}\frac{\sqrt{3}}{2}f_+f_- \end{vmatrix} = 0.$$

---

the perpendicular plane [1,2] (For that mode the number of "short legs" Mn − O equals four and the "long" ones equals two.) These deformations are also seen in some doped materials (*e.g.* see in [22]). Alternations of that specific type would be reflected in expression (7) as changes from $\theta = 2\pi/3$ to $\theta = -2\pi/3$ between the two sublattices. That will lead to the band's secular equation which can not be solved in the analytic form. However, one can consider the contribution, which comes from the Q_2 mode only; this deformation just changes the sign on the adjacent sites of two sublattices, as also follows from the equation (8) and Figure 1. For that pattern one may easily right down $\hat{H}_{\mathrm{JT}}$ as:

$$\begin{aligned} \hat{H}_{\mathrm{JT}}(\mathbf{q}) &= -\frac{gQ_0}{2}\exp(\mathrm{i}\mathbf{qr})\begin{pmatrix} 0 & 1 \\ 1 & 0 \end{pmatrix} \\ &= -\frac{gQ_0}{2}\exp(\mathrm{i}\mathbf{qr})\hat{\tau}_x \end{aligned} \tag{21}$$

and obtain the spectrum by following the line of our reasoning used above, when we were deriving the equations (16, 17) ($\hat{\tau}_x$ is a "pseudospin" Pauli matrix defined on the basis (5)).

Writing explicitly

$$\begin{aligned} \left[\,\hat{\varepsilon} - \hat{t}(\mathbf{p})\,\right]\psi_{\mathbf{p}} &= -\frac{gQ_0}{2}\,\hat{\tau}_x\,\psi_{\mathbf{p+q}}, \\ \left[\,\hat{\varepsilon} + \hat{t}(\mathbf{p})\,\right]\psi_{\mathbf{p+q}} &= -\frac{gQ_0}{2}\,\hat{\tau}_x\,\psi_{\mathbf{p}} \end{aligned} \tag{22}$$

(by definition $\hat{t}(\mathbf{p}+\mathbf{q}) = -\hat{t}(\mathbf{p})$). Eliminating $\psi_{\mathbf{p+q}}$ from equation (22), one obtains:

$$\left[\varepsilon\,\hat{\tau}_x + \hat{\hat{t}}(\mathbf{p})\right]\left[\varepsilon\,\hat{\tau}_x - \hat{\hat{t}}(\mathbf{p})\right](\hat{\tau}_x\,\psi_{\mathbf{p}}) = \left(\frac{gQ_0}{2}\right)^2\hat{\tau}_x\,\psi_{\mathbf{p}}.$$

The spectrum branches are then obtained from the zeroes of the two-by-two determinant:

$$\det\left|\left(\varepsilon^2 - \frac{gQ_0}{2}^2\right)\hat{e} - \hat{\hat{t}}(\mathbf{p})^2 + \varepsilon\left[\hat{\hat{t}}(\mathbf{p}),\ \hat{\tau}_x\right]\right| = 0, \tag{23}$$

where $\hat{e}$ is the unit matrix, $\hat{\hat{t}}(\mathbf{p}) = \hat{t}(\mathbf{p})\,\hat{\tau}_x$, and

$$\left[\hat{\hat{t}}(\mathbf{p}),\ \hat{\tau}_x\right] = \hat{t}(\mathbf{p}) - \hat{\tau}_x\,\hat{t}(\mathbf{p})\hat{\tau}_x. \tag{24}$$

With $\hat{t}(\mathbf{p})$ expressed in terms of the "pseudospin" Pauli matrices:

$$\hat{t}(\mathbf{p}) = -f_+(\mathbf{p})\hat{e} + \frac{1}{2}f_+(\mathbf{p})\hat{\tau}_x + \frac{\sqrt{3}}{2}f_-(\mathbf{p})\hat{\tau}_y, \tag{25}$$

where $f_+(\mathbf{p}) = \mid A \mid (c_x + c_y), f_-(\mathbf{p}) = \mid A \mid (c_x - c_y)$, after simple calculations, determinant (23) transforms to the form:

see equation above.

The resulting bi-quadratic equation produces the following four branches, $\varepsilon_i(\mathbf{p})(i = 1...4)$. Each of these four branches is determined in the reduced Brillouin zone:

$$\begin{aligned} \varepsilon_{1,2}(\mathbf{p}) &= \left\{(gQ_0/2)^2 + \frac{5}{4}f_+^2 + \frac{3}{4}f_-^2\right. \\ &\qquad \left.\pm\sqrt{3f_-^2\left[(gQ_0/2)^2 + f_+^2\right] + f_+^4}\right\}^{1/2} \\ \varepsilon_{3,4}(\mathbf{p}) &= \left\{(gQ_0/2)^2 + 5/4f_+^2 + 3/4f_-^2\right. \\ &\qquad \left.\pm\sqrt{3f_-^2\left[(gQ_0/2)^2 + f_+^2\right] + f_+^4}\right\}^{1/2}. \end{aligned} \tag{26}$$

At large enough $|gQ_0/2\ |$ the branches $\varepsilon_{1,2}(\mathbf{p})$ are not crossing two other branches, $\varepsilon_{3,4}(\mathbf{p})$. Filling them up by two polarized electrons per doubled unit cell, completes the proof that, indeed, insulating $\mathrm{LaMnO_3}$ may be considered as *band* insulator.

For example, two sets of the spectrum branches (26), $\varepsilon_{1,2}(\mathbf{p})$ and $\varepsilon_{3,4}(\mathbf{p})$ begin to overlap for $\varepsilon_{j=1}(\mathbf{p})$ and $\varepsilon_{i=3}(\mathbf{p})$ at $p_x = p_y = \pi/2$. The overlap is direct which imposes some limit on the value of the JT mode which makes $\mathrm{LaMnO_3}$ to be an insulator:

$$|gQ_0| > 0.1|A|. \tag{27}$$

The optical gap, hence, corresponds to excitation of an electron from the $\varepsilon_{j=1(2)}(\mathbf{p})$ band into the $\varepsilon_{i=3(4)}(\mathbf{p})$.

The optical spectra would, in principle, allow to access the gap directly. The detailed analysis of the optical absorption in the pure $\mathrm{LaMnO_3}$ may be further complicated by the fact that formation of an electron-hole pair by light, strictly speaking, should not lead to creation of individual electron- and hole-like excitations due to inevitable polaronic effects in the *ionic* crystal $\mathrm{LaMnO_3}$. Since the experimental level of current optical studies (see [11]) in $\mathrm{LaMnO_3}$ can not address the issue yet, we shall not dwell upon further theoretical analysis.

To complete this section, one more simple comment may be helpful. Namely, while in the case of a single ion with one electron occupies the *local* degenerate e_{2g}-level, it inevitably leads to the local instability caused by the linear JT term (4), the ferromagnetic state with the band spectrum (13), filled up to some level, would remain stable with respect to *small* enough JT distortions. There is a *threshold value* for the magnitude of the JT-terms, before the distorted JT state may set in. This threshold is determined by the electronic kinetic energy gain and the elastic lattice energy. In case of $\mathrm{LaMnO_3}$ the existence of the cooperative JT deformations is confirmed experimentally.

5 Doped manganites. Percolation

With the substitutional doping, $A_{1-x}B_xMnO_3$, say in, $La_{1-x}Sr_xMnO_3$ by Sr, the materials initially show no metallic behavior with resistivity increasing by many orders of magnitude at $T \geq 0$, In metals, one would expect that resistivity behaves like

$$\rho(T) = \rho_0 + AT^{\alpha}, \tag{28}$$

where ρ_0, the residual resistivity, is due to the structure defects or impurities, while the T-dependence comes up from scattering on thermal phonons or from electron-electron interactions. In the second case, the electronic relaxation rate $1/\tau_{\mathrm{ee}} \sim T^2/E_{\mathrm{F}}$, while the phonon mechanism prevails at $1/\tau_{\mathrm{ph}} \sim T^3/\theta^2 > 1/\tau_{\mathrm{ee}}$, *i.e.* at $T > \theta(\theta/E_{\mathrm{F}})$, where θ is the characteristic phonon frequency. The latter in manganites is about four hundred degrees Kelvin while, as we will see, for E_{F} in manganites one gets the scale $E_{\mathrm{F}} \sim 0.1$ eV. Hence, the electron mechanism might become important up to rather high temperatures. However, at elevated temperatures a lot of new effects, related to the colossal magnetoresistance phenomenon, start to play the dominating role.

To understand the nature of the ground state of pure and doped manganites, we need,first of all, to concentrate our attention on the low temperature properties. It has been shown first in [28] that low T resistivity changes its character with doping, so that the metallic behavior (28) sets in at $x = x_{\mathrm{cr}} \approx 0.16 - 0.17$ [24,25]. Interestingly enough, the onset of conducting regime coincides with the onset of the low temperature ferromagnetism, strongly indicating in favor of DE mechanism for the latter.

The value of ρ_0 may vary, even for nominally the same material and composition, implying that quality of samples may need further improvement. At the same time it is clear, that in all cases the change from insulating to metallic behavior takes place when x is close to the critical concentration, x_{cr}.

The origin of that threshold and its value have been first understood in [9,14] in terms of percolation theory (for review on percolation theory see *e.g.* the book [26]). The latter considers any process which, roughly speaking, corresponds to some exchange between two adjacent local sites. A material, $A_{1-x}B_xMnO_3$, is commonly prepared by various methods at high temperatures. As the result, position of atom B, which is a substitution for a parent atom, is completely random. Divalent atom B, locally creates a "hole" on adjacent Mn-sites which could serve as a charge carrier if there were no long range Coulomb forces in the dielectric phase, which keep the "hole" close to the negative charge at B^-. When concentration is small, average distances between B atoms are large, which makes holes remain isolated. In the theory of percolation one may look for the concentration at which the nearest neighbor B-atoms start to form infinite clusters piercing the whole crystal. For the B-atoms on the cubic sites it is known as the "site" problem: on the simple cubic lattice it gives the critical concentration value at ~ 0.31. However, this is not exactly our case. For the doped holes, gathering on few manganese sites around an atom B, charge transfer takes place only along Mn-O-Mn bonds. Therefore the picture of a critical cluster, constructed from the B^--ions must be corrected: such cluster would already have a finite "thickness" due to the holes spread over surrounding Mn-sites. Numerical studies on the percolative models [27] have shown that this circumstance (*i.e.* the presence of the scale of a few lattice constants) strongly decreases the value for the critical concentration, rapidly converging to its value for the homogeneous problem, $x_{\mathrm{cr}} \sim 0.16$. The phenomenon of percolation in disordered media is akin to the other critical phenomena: it bears a singular behavior in the vicinity of x_{cr}, $|x - x_{\mathrm{cr}}| \ll x_{\mathrm{cr}}$. Thus, it is expected that conductivity above x_{cr} or $\rho_0^{-1}(x)$ in (21) should behave as $\sigma(x) \propto (x - x_{\mathrm{cr}})^{\gamma}$, where γ is a critical index. There were not many attempts to verify singular behavior in conductivity. The data [28,29] are consistent with the index $\gamma \sim 0.5 - 0.6$ [22].

The above arguments have been given at $T = 0$. One may try to apply similar ideas to the CMR phenomena at $T = T_{\mathrm{c}}$ (see, *e.g.*, in [9,14]). Indeed, if resistivity, $\rho(T > T_{\mathrm{c}})$ is large enough, as it usually is, one may approximately take the *conductivity*: $\sigma(T > T_{\mathrm{c}}) = \rho^{-1}(T > T_{\mathrm{c}}) \simeq 0$. The fast increase in $\sigma(T)$ at $T < T_{\mathrm{c}}$ is then expected to correspond $\sigma(T < T_{\mathrm{c}}) \propto (T_{\mathrm{c}} - T)^{\overline{\gamma}}$. This is approximately true for $La_{0.8}Sr_{0.2}MnO_3$ near T_{c} with $\overline{\gamma} \sim 0.6$ [23].

The correctness of the percolation theory views may be also verified by independent measurements of $\sigma(T, x)$ and magnetization, $M(T, x)$, or $D_{\mathrm{stiff}}(T, x)$ – the so-called "spin-stiffness" which determines the spectrum of the long-wave magnons:

$$\omega(\mathbf{k}) = D_{\mathrm{stiff}}\mathbf{k}^2 \tag{29}$$

(D itself is proportional to M). The Kirkpatrick's relation gives:

$$\sigma \propto DM. \tag{30}$$

Equation (30) may be verified at x close to x_{cr} or at T near T_{c}.

For percolation in the continuous phases description the physical picture is rather well understood. One of the helpful observations is that for the three-dimensional problem there is a concentration range in which percolation (infinite clusters) may take place simultaneously for two phases (insulating and conducting, for instance) though taking into account the surface tension at the boundary between two phases seems to impose limitations on relative thickness of the phases.

In case of manganites, understanding on the microscopic level remains far from being complete, though the concept is by all means correct. In the above, the mixture of "two" phases, depending on the concentration, x, may look as intervened tiny "islands" and "layers" of different "phases", whose thickness even difficult to access quantitatively. Well below and well above the threshold concentration x_{cr}, one may imagine each corresponding phase as a bulk formation into which the second phase is sparsely embedded. If there is a spill-over of charge carriers between two phases, it is the electro-neutrality condition which regulates the tiny domain sizes.

6 Physical properties in two-band model

As it was explained in the previous Section, the percolation being a critical phenomenon, may cede soon to the onset of the homogeneous ferromagnetic phase, when screening becomes effective. In fact, some good samples of $La_{1-x}Sr_xMnO_3$ show low temperature resistivity in the range $10^{-4} - 10^{-5}(\Omega - \mathrm{cm})$ [45]. Interest in applications of CMR was the main reason why the properties of manganites with $x \sim 0.3$ have been elaborated rather carefully (temperature of the resistivity peak, T_p, reaches its maximum at 300 K for concentrations in this range). There are still indications [22] that remnants of the second phase may still persist at $x \sim 0.3$. However, below we will analyze available low temperature experimental data for doped manganites from the band approach. Our conclusions will be that the band model (or Fermi liquid) approach seems to be valid at low temperatures, especially for the high quality samples. Data are hindered by sample's quality with local inhomogeneities or the second phase inclusions forming the scattering centers. For a number of compositions, depending on tolerance factor, conductivity is close to its value in the mobility edge regime. The two band model, thus, turns out to be a good starting point even at given doping level, providing together with the interpretation of the parent material, $LaMnO_3$, an avenue for unifying theoretical understanding of the manganites properties.

Making use of the spectrum (13), we calculate the concentration dependence of the Fermi-level, $E_\mathrm{F}(x)$, the density of states (DOS), $\nu(x)$, the spin stiffness, $D(x)$, and the whole magnon spectrum, $\omega(\mathbf{k}, x)$, and the conductivity, $\sigma(\omega, x)$, both the Drude and the optical (interband) components. Theoretical results depend only on the single hopping integral, $|A|$.

We start with the calculations of the spin wave spectrum. Let us write the deviations from the average spin, $\langle S_z\rangle$ for the localized t_{2g}-spins ($\mathbf{s} = \mathbf{S} - \langle S_z\rangle$) as:

$$\begin{aligned} s^+(\mathbf{q}) = (2\langle S_z\rangle)^{1/2}\ \hat{b}(\mathbf{q}),\ s^-(\mathbf{q}) = (2\langle S_z\rangle)^{1/2}\hat{b}^+(\mathbf{q}),\\ s_z(\mathbf{q}) = (\hat{b}^+\hat{b})_\mathbf{q}, \end{aligned} \tag{31}$$

($\hat{b}^+, \hat{b}$ – the magnon's operators). The first (δE_1) and second (δE_2) order corrections to the ground state are calculated as perturbations in:

$$\hat{V} = -J_\mathrm{H}\sum_i \mathbf{s}_i(\hat{a}_i^+\boldsymbol{\sigma}\hat{a}_i) = -J_\mathrm{H}\sum_i \mathbf{s}_i\mathbf{n}_i. \tag{32}$$

For δE_2, the matrix elements in (32) are of the form:

$$\begin{aligned} V^{l,l'}_{\mathbf{p}-\mathbf{k},\uparrow;\mathbf{p}\downarrow} = -J_\mathrm{H}\langle\uparrow|s^\pm(\mathbf{k})|\downarrow\rangle\\ \times\left(\alpha^l_{\mathbf{p}-\mathbf{k}}\alpha^{*l'}_\mathbf{p} + \beta^l_{\mathbf{p}-\mathbf{k}}\beta^{*l'}_\mathbf{p}\right), \end{aligned} \tag{33}$$

(the coefficients $\alpha^l_\mathbf{p}, \beta^l_\mathbf{p}$ are defined below). As for δE_1, its only role is to secure the proper behavior of the magnon spectrum at $k \to 0$). One obtains:

$$\begin{aligned} \delta E_2 = 2J_\mathrm{H}^2\sum_\mathbf{k}\langle S_z\rangle\hat{b}^+(\mathbf{k})\hat{b}(\mathbf{k})\\ \times\sum_{l,\mathbf{p}}\left(\sum_{l'}\frac{|\alpha^l_\mathbf{p}\alpha^{*l'}_{\mathbf{p}+\mathbf{k}} + \beta^l_\mathbf{p}\beta^{*l'}_{\mathbf{p}+\mathbf{k}}|^2}{E^l_\uparrow(\mathbf{p}) - E^{l'}_\downarrow(\mathbf{p}+\mathbf{k})}\right), \end{aligned} \tag{34}$$

where

$$E^{l,l'}_{\uparrow,\downarrow}(\mathbf{p}) = \mp J_\mathrm{H}\langle S_z\rangle + \varepsilon_{l,l'}(\mathbf{p}). \tag{35}$$

Both sums in (34) run over $l, l' = \pm$ (Eq. (13)). The summation over l and $\mathbf{p}$ is limited by the occupied states (↑) only. The coefficients $(\alpha^l_\mathbf{p}, \beta^l_\mathbf{p})$ above are for the Bloch's states on the basis (5):

$$\alpha^{l,l'}_\mathbf{p} = (\Sigma_{12}/2|\Sigma_{12}|)^{1/2},\ \beta^{l,l'}_\mathbf{p} = \pm(\Sigma_{21}/2|\Sigma_{12}|)^{1/2}, \tag{36}$$

(here Σ_{12}, Σ_{21} are the off-diagonal elements of the hopping matrix $\hat{t}(\mathbf{p})$ in (11) on this basis).

Assuming in (34, 35) (recall that $J_\mathrm{H} \gg |A|$ ($J_\mathrm{H}S_z$ is of the order of 1.5 eV [1] , while estimates below produce for $|A| \sim 0.1$ eV), expanding (34) in $|A|/J_\mathrm{H}$ would get a series of the Heisenberg spin Hamiltonians accounting for interactions with the increasing number of neighbors. (For a single band it was first noticed in [30]; in this paper we are using the realistic two bands picture.) After a somewhat tedious, but straightforward calculation, the first order term in $|A|$ from (34) is ($\langle S_z\rangle = 3/2$):

$$\hbar\omega(\mathbf{k}) = |A|(3 - c_x - c_y - c_z)D(x)/3 \tag{37}$$

and $D(x) \equiv D(E(x))$ is given by the integral:

$$\int\frac{\mathrm{d}^3\mathbf{p}}{(2\pi)^3}\left[\sum_{(+,-)}\theta(E - \varepsilon_i(\mathbf{p}))\left\{1 \pm \frac{2c_x - c_y - c_z}{2R(\mathbf{p})}\right\}\right],$$

(here E is in units of $|A|, p_i \equiv ap_i$). Quantum fluctuations may change the $\mathbf{k}$-dependence in equation (37).

Let us turn now to the calculation of conductivity, $\sigma_{ij}(\omega, x)$, which is described by:

$$\begin{aligned} \sigma_{ij} = -\frac{e^2\hbar^2}{V\omega}\sum_{\mathbf{k},\mathbf{k}'} f_0(\mathbf{k})\left[1 - f_0(\mathbf{k}')\right]\\ \times\langle\psi(\mathbf{k})\mid\hat{v}_i\mid\psi(\mathbf{k}')\rangle\langle\psi(\mathbf{k}')\mid\hat{v}_j\mid\psi(\mathbf{k})\rangle\\ \times\left[\delta(\epsilon(\mathbf{k}') - \epsilon(\mathbf{k}) - \omega) - \delta(\epsilon(\mathbf{k}') - \epsilon(\mathbf{k}) + \omega)\right], \end{aligned} \tag{38}$$

where $f_0(\mathbf{k})$ is the Fermi distribution function, $\mathbf{k}$ is a quasi momentum, $\hat{v}_i$ is a velocity operator. For the cubic crystal $\sigma_{ij} = \sigma_{ji}$.

We determine first the velocity operator, $\hat{\mathbf{v}} = \dot{\hat{\mathbf{r}}}$ (see [31]):

$$\hat{\mathbf{v}}(\mathbf{k}) = \frac{1}{\hbar}\frac{\partial\varepsilon_l(\mathbf{k})}{\partial\mathbf{k}} + \frac{\mathrm{i}}{\hbar}[\varepsilon_l(\mathbf{k}) - \varepsilon_{l'}(\mathbf{k})]\,\langle l\mathbf{k}|\hat{\boldsymbol{\Omega}}|l'\mathbf{k}\rangle. \tag{39}$$

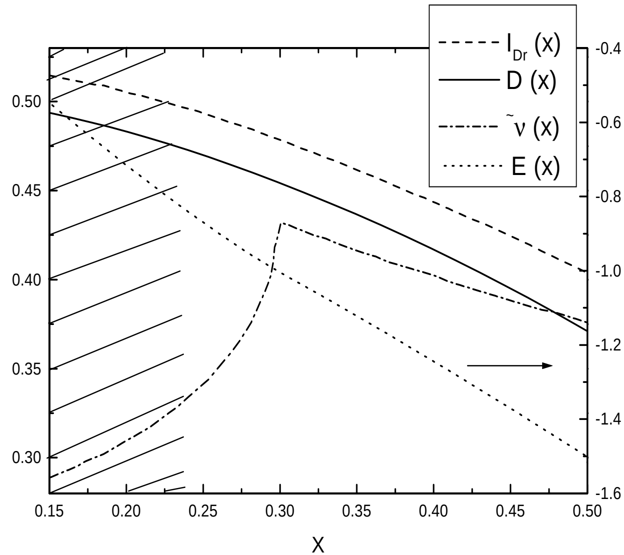

Fig. 2. The Fermi level, $E(x)$, DOS, $\tilde{\nu}(x)$, the spin stiffness coefficient $D(x)$ and the Drude conductivity, $I_{\rm Dr}(x)$, plotted as a function of concentration, x, for the spectrum, given in [20]. The shaded area shows the percolative regime where equations (37-46) are not applicable.

The off-diagonal operator $\hat{\boldsymbol{\Omega}}$ is defined by the relation:

$$\langle l\mathbf{k}|\hat{\boldsymbol{\Omega}}|l'\mathbf{k}\rangle = \mathrm{i}\int u^{*l'}_{\mathbf{k}}(\mathbf{r})\frac{\partial u^l_{\mathbf{k}}}{\partial \mathbf{k}}\mathrm{d}^3\mathbf{r} \tag{40}$$

and $u^l_{\mathbf{k}}(\mathbf{r})$, the periodic Bloch functions on the basis of equation (5) are:

$$u^l_{\mathbf{k}}(\mathbf{r}) = \frac{1}{\sqrt{N}}\sum_n \exp[\mathrm{i}\mathbf{k}(\mathbf{a}n - \mathbf{r})] \times \left\{\alpha^l_{\mathbf{k}}\phi_1(\mathbf{r} - n\mathbf{a}) + \beta^l_{\mathbf{k}}\phi_2(\mathbf{r} - n\mathbf{a})\right\}. \tag{41}$$

With the one-site integrals only in (40) and equations (36):

$$\langle l\mathbf{k}|\hat{\boldsymbol{\Omega}}|l'\mathbf{k}\rangle = \mathrm{i}\frac{a}{\hbar}\frac{\sqrt{3}}{4}\frac{(-\sin k_x)(c_y - c_z)}{|t_{12}|^2}\,\cdot \tag{42}$$

Matrix elements in (39, 42) produce transitions from *occupied* parts of the $\varepsilon_+(\mathbf{p})$-band into *empty* states in the $\varepsilon_-(\mathbf{p})$-band.

With all the above, we arrive to the Drude (intraband) contribution which in the clean limit is:

$$\sigma_{\rm Drude}(\omega, x) = 2\pi\frac{e^2|A|}{3a\hbar^2}\delta(\omega)I_{\rm Dr}(x), \tag{43}$$

$$I_{\rm Dr}(x) = \frac{1}{2(2\pi)^3}\sum_l\int \mathrm{d}S^l_{\mathbf{p}}|\boldsymbol{\nabla}_{\mathbf{p}}\varepsilon(\mathbf{p})|, \tag{44}$$

(the integral in $I_{\rm Dr}(x)$ is over the Fermi surfaces).

The "optical" (interband) contribution is

$$\sigma_{\rm opt}(\omega, x) = \frac{3\pi e^2}{a\hbar}\frac{1}{\tilde{\omega}_0^3}\int\frac{\mathrm{d}^3\mathbf{p}}{(2\pi)^3}\sin^2 p_x(c_y - c_x)^2 \times\ n(\varepsilon_+(\mathbf{p}))[1 - n(\varepsilon_-(\mathbf{p}))]\delta\left(\tilde{\omega} - 2R(\mathbf{p})\right), \tag{45}$$

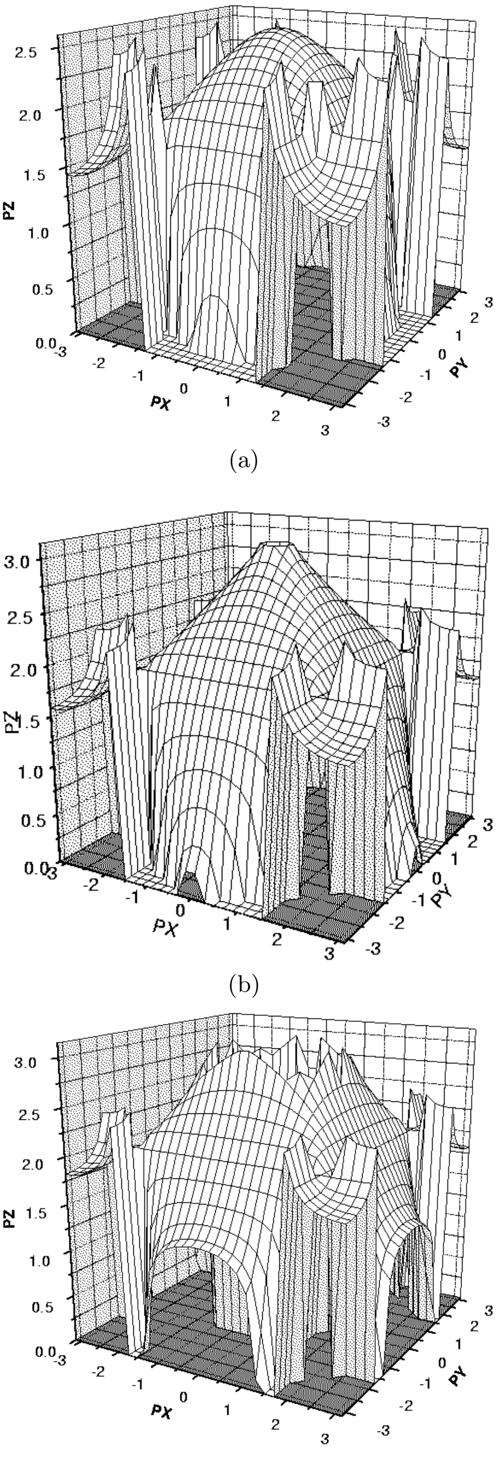

(a)

(b)

(c)

Fig. 3. The Fermi surface (a) $x = 0.2$; (b) $x = 0.3$; (c) $x = 0.5$.

where $|A|\tilde{\omega} = \hbar\omega$ (Eqs. (44) and (45) agree with the similar calculations of [32]). For the low temperature spectral weight

$$N_{\rm eff} = \frac{2m}{\pi e^2}a^3\int\limits_0^\infty \sigma(\omega)\mathrm{d}\omega \tag{46}$$

one obtains both the Drude and the interband contributions, respectively:

$$N_{\rm eff}^{\rm Drude} = \frac{ma^2}{3\hbar^2}|A|I_{\rm Dr}(x),\ N_{\rm eff}^{\rm opt} = \frac{ma^2}{\hbar^2}|A|\frac{3}{4}I_{\rm opt}(x), \tag{47}$$

(with $I_{\rm opt}(x)$ directly obtained from (45)). In Figure 2 we plotted our results for the Fermi level, $E_{\rm F}(x) = |A|E(x), \tilde{\nu}(x) = \nu(x)|A|, D(x)$ and $I_{\rm Dr}(x)$ (the shaded area shows schematically the concentration range for a percolative regime). In Figure 3 evolution of the Fermi surface with x is shown (Fermi surfaces in Figs. 3a, b, c are for concentrations $x = 0.2, 0.3, 0.5$ respectively.) An interesting fact is that $x = 0.3$ is the concentration at which a "neck" develops at the zone boundary of the Fermi surface. In other words, concentration $x = 0.3$ is the point of "2.5"-Lifshitz transition at which the change in the Fermi surface topology occurs.

7 The model and experiment. Discussion

In the discussion below we restrict ourselves mainly by the "isotropic" materials, *i.e.* by the range of concentrations $x \leq 0.4$. Around $x \sim 0.5$ new phenomena start to develop in doped manganites, such as charge ordering [33,34], A-phase in $\rm Pr_{0.5}Sr_{0.5}MnO_3$ and $\rm Nd_{0.45}Sr_{0.55}MnO_3$ [35,36], structural transitions caused by magnetic field in $\rm Pr_{0.5}Sr_{0.5}MnO_3$, $\rm Nd_{0.5}Sr_{0.5}MnO_3$ [37–39,41] and "spin valve" effect in $\rm Nd_{0.46}Sr_{0.54}MnO_3$ [40]. Though some preparatory steps have been made to address these issues, *e.g.* equations (14, 14') in Section 3, the purpose of this paper is mainly to access the limits of applicability of the band structure theory above, and its parameters. For these reasons the concentration range $x \sim 0.3$ is chosen where more data are available. A word of caution still would be helpful. Although the quality of materials has been dramatically improved for the past couple of years and many results are becoming quite reproducible, systematic studies of the same phenomenon on the same materials, which would have been performed in different laboratories, are rather rare. It is also not well known how data, obtained on single crystals may differ from the ones obtained in crystalline films.

The spectrum (13) and the results above, such as (37, 43-47) include the single energy scale, $|A|$. We choose to determine this parameter from the measured spin stiffness coefficient in (37):

$$\hbar\omega(\mathbf{k}) = \frac{(\mathbf{ka})^2}{6}|A|D(x), \tag{38'}$$

i.e.

$$D_{\rm stiff} = \frac{a^2}{6}|A|D(x).$$

Being a long-wave characteristics, a latter must be less sensitive to defects of sample's quality. We use $a \simeq 3.86$ Å, $D(x \simeq 0.3) \simeq 0.45$ (according to our results in Fig. 2) and the data, collected in [42] (Tab. 1). The results for $|A|$ show that the bandwidths for different materials, $W = 6|A|$, do not vary significantly ($W \simeq 0.7$–1.0 eV). This is in favor of the fact that the tolerance factor itself which is responsible for variations in the $\rm Mn - O - Mn$ bonds angle for the different materials, is *not* of much importance, as it has already been suggested for the bandwidth in [20,22]. As for the concentration dependence, $D(x)$ in Figure 2, it reflects the fact that number of electrons and, hence, the saturation moment $M(x)$ decreases with the increase of x. There are measurements of $D_{\rm stiff}(x)$ [43,44] which show some pronounced dependence on $x < 0.2$ and saturation at $x = 0.28, 0.3$ [43]. The decrease in $D(x)$, according to our results, shown in Figure 2, at $x \sim 0.3$ is below the experimental accuracy in [43]. As for measured dependence $D_{\rm stiff}(x)$ for smaller concentrations, here one may meet the range for the percolative behavior, shown in our Figure 2 by the shaded area. We will return to it later, although it is worth mentioning that data [43,44] do not agree with each other above $x = 0.2$.

With $|A| \simeq 0.16$ eV ($\rm La_{1-x}Sr_xMnO_3$) one may find the thermodynamical parameters and the density of states, $\nu(x) = \tilde{\nu}(x)/|A|$. Correspondingly, the Sommerfeld coefficient, γ, for our spectrum (13) is

$$\gamma = \pi^2\tilde{\nu}(x)/3|A|. \tag{48}$$

An attempt to investigate properties of $\rm La_{1-x}Sr_xMnO_3$ systematically has been done by Okuda, where special efforts were applied to single out the electronic component into the specific heat by subtracting both phonon and magnon contributions. According to [24], $\gamma \simeq 3.5$ mJ/mole K^2, while $\tilde{\nu}(x) \simeq 0.45$ at $x = 0.3$ from Figure 2 produces $\gamma \simeq 6.2$ mJ/mole K^2. Note, however, that $\tilde{\nu}(x)$ has a kink at $x = 0.3$. That kink takes its origin from the fact that this concentration is the point of the Lifshitz singularity, as it may be clearly seen from the Fermi surface pattern in Figure 3. The total magnon contribution into specific heat is proportional to $T^{3/2}$. The proximity to the Lifshitz "2.5" transition results in appearance of the same T-dependence of the electronic specific heat. As the result, the procedure, [24], of extracting magnon $T^{3/2}$ terms becomes less transparent. It is worth mentioning that unambiguous determination of the electronic contribution is known [1] as a difficult task. The low T electronic specific heat of a few other manganite compounds has also been measured with γ in the 3–8 mJ/mole K^2 range. Taking into account the possible complications with the rapid energy dependence in the density of states close to $x = 0.3$, the accuracy of equation (48) seems to us rather satisfactory.

Important issue is a sensitivity of all data to disorder, which is inevitably present at the substitutional doping. The concentrations are not small by all means. The residual resistances in equation (28) obtained for nominally the same compositions, may vary significantly for different groups of compounds. So, it is clear, that to some extent, the best values of $\rho_0(x)$ are still to be determined. Meanwhile, it remains unclear whether $\rho_0(x)$ only characterizes the sample's quality or there is an intrinsic component in the residual resistance. In favor of the former suggestion tells the results of recent experiments performed by [19,45,46]. New records have recently been reported for conductivity, measured in a few compounds. Among them there are resistivity data for $La_{1-x}Sr_xMnO_3$ in crystalline films which give the value for $\rho_0(x)$ as low as 10^{-5} Ωcm [45]. This is a typical metallic conductivity range. Making a substitution in equation (43) for $\pi\delta(\omega) -> \tau/(1+(\omega\tau)^2)$, we obtain in this case $\hbar/\tau|A| \sim 2 \times 10^{-2}$, *i.e.* for the inverse life time, $\hbar/\tau \sim 3 \times 10^{-3}$ eV($\sim$ 30 K). At the same time the residual resistivity for other materials studied in [45], lie in the range $100 \div 300(\mu\Omega-$cm), *i.e.* $\hbar/\tau|A| \sim 0.5$. These findings become more transparent being expressed in terms of the mean free path. With the average velocity of an electron on the Fermi surface

$$\overline{v} = \langle \mathbf{v}^2 \rangle^{1/2} = (|A|a/\hbar)(2I_{\mathrm{Dr}}(x)/\tilde{\nu}(x))^{1/2}, \tag{49}$$

the mean free path, $l = \overline{v}\tau$, is typically $\sim 3a$ for materials with $\rho_0 \sim 10^{-4}$ (Ω cm), while in the best LSMO samples it is around $80a$. Whether the values of ρ_0 mentioned above may be or may be not improved by a more careful sample preparation process, remains to be seen. In any case, for some current materials [45] the conductivity regime lies close to the mobility edge. If the short mean free path in these materials is an intrinsic feature, it may be related to the local fluctuations in the tolerance factor (1) caused by the difference in ionic radii at the Sr-substitution. Indeed, with $\langle r_0 \rangle = 0.14$ nm, $\langle r_{\mathrm{Sr}} \rangle = 0.129$ nm, $\langle r_{\mathrm{La}} \rangle = 0.136$ nm for Pr^{3+} and Nd^{3+} one has $\langle r_{\mathrm{Pr}} \rangle = 0.129$ nm and $\langle r_{\mathrm{Nd}} \rangle = 0.124$ nm [1] (p. 194). As it has been emphasized already, our two-band approach is a simple way of the Fermi liquid description, when interactions are not supposed to be remarkably strong. The strength of interactions is provided by the T^2-term in resistivity, in which electron interactions come from $\hbar/\tau_{\mathrm{ee}}^{\mathrm{tr}} = \lambda' (\hbar/\tau_{\mathrm{ee}})$, where τ_{ee} is the total quasiparticle relaxation time and $\lambda' < 1$ gives the fraction of Umklapp processes. We use [47]:

$$\hbar/\tau_{\mathrm{ee}} \simeq \lambda\pi^3\nu(x)T^2. \tag{50}$$

In (50) λ is a value of the interaction strength in terms of E_{F}. Using [45,46], one obtains for LSMO: $\lambda\lambda' \simeq 0.3$, typical of good metals. As for the two other materials in [45], the T-variations of resistivity scale in the magnitude with their residual resistivity and most probably are caused by defects [48].

T-dependence in the optical conductivity, $\sigma(\omega)$, attracted recently much attention [24,45,49] as a manifestation of changes in the conductivity mechanism from metallic to localized polarons at elevated temperatures. We discuss only a few results pertinent to the low T band mechanisms. First note, that the temperature dependence in $\sigma(\omega)$ at $T < 100$ K for ω around 1 eV is most pronounced *below* 1 eV (see Fig. 2 in [45]). This agrees well with our estimates for the bandwidths, $W \leq 1$ eV. As for a quantitative analysis, there are problems of an experimental character. Assuming $N_{\mathrm{eff}}(\omega)$ [45] would give our N_{eff}'s in equation (47) at $\omega \simeq 1$ eV and that both the Drude and optical contributions are approximately equal [32], we obtain $N_{\mathrm{eff}} \sim 0.25$ which is reasonably close to the values in [45] , lesser than N_{eff} for the single crystal data, $La_{0.67}Ca_{0.33}MnO_3$ [49] , and a factor ten bigger than N_{eff} for $La_{0.7}Sr_{0.3}MnO_3$ in [11] . We believe that such a difference originates from poor data for the optical $\sigma(\omega)$ in the "Drude-tail" range.

Finally, the optical gap for pure $LaMnO_3$ was identified [11] at $\Delta \simeq 1.2$ eV. A rough estimate from the band insulator picture (26) gives $gQ_0/2 \sim 0.6$ eV, *i.e.* the JT-coupling is rather strong ($|A|{\sim}0.16$ eV).

We conclude the discussion by a few comments regarding the spin wave spectrum. In $La_{0.7}Pb_{0.3}MnO_3$ [50] the spectrum fits well (37). Equation (37) follows from (34) at $A \ll J_{\mathrm{H}}\langle S_z \rangle$, with quantum corrections neglected (we have also neglected terms of the order of t^2/J_{H}). Meanwhile, strong deviations from (37) have been observed at $\xi > 0.25$ along the (0,0,ξ)-direction in $Pr_{0.63}Sr_{0.37}MnO_3$ [51]. The spin stiffness changes only slightly from material to material [50], and other low temperature characteristics including strength of electron interactions, also seem not to vary much. Unlike [50], we suggest with [51] that differences in low-T spin dynamics for two materials do not correlate with their behavior at higher temperatures, but with a tendency to a low temperature charge ordering or formation of the A-phase at x close to 0.5 (we will address this issue elsewhere).

Let us now return to the problem of how doped manganites proceed from the insulating end, $LaMnO_3$, with the increase of concentration, x. At $x < x_{\mathrm{cr}}$ doped holes remain localized in the vicinity of corresponding clusters. If the clusters are small enough they might be called "ferromagnetic polarons" but this is a semantics. In [52] it has been argued that such isolated microscopic ferromagnetic inclusions do produce a macroscopic consequences, forming "canted" ferromagnetic moment even in the A-phase of parent $LaMnO_3$. In other words, the effective radius of ferromagnetic interactions is larger than short range coupling in the percolative scenario for conductivity. The relation (30) based on the assumption of equal effective radii both for conductivity hopping and ferromagnetic interactions, is, thus, not expected to be applicable near $x_{\mathrm{cr}} = 0.16$: magnetic ordering and ferromagnetic component in the spin waves, may develop earlier. The experimental results [43,44], indeed, show the stiffness coefficient, $D_{\mathrm{stiff}}(x)$ nonzero below x_{cr} and starting to increase almost at $x < 0.15$. However, the further sharp increase above $x_{\mathrm{cr}} = 0.16$ with a saturation near $x \simeq 0.3$, is the bright demonstration in favor of the notion of percolation: the increase in $D_{\mathrm{stiff}}(x)$ just follows increase in the amount of the ferromagnetic component. Note, that $D_{\mathrm{stiff}}(x)$ is proportional to the value of magnetization, $M(x)$. In the band picture, $M(x)$ is $(4-x)\mu_{\mathrm{B}}$. As it is known since the old results [1] that $M(x)$ actually increases at $x > 0.1$. Interesting thing is that $M(x)$ has dependence, close to $(4-x)\mu_{\mathrm{B}}$, even at $x \sim 0.3$–0.4, indicating that admixture of "insulating phase" still persists at these concentrations.

Another proof comes from recent pulsed neutron experiments [22,53]. These experiments probe the local arrangement of the oxygen octahedra. With the random disorder, one may expect that the degeneracy of the e_{2g}-terms would also be lifted randomly, providing a distribution in the JT deformations of the oxygen octahedra. Meanwhile, it has been shown in [22] that the pair distribution function displays the well pronounced peaks at the values of $\mathrm{Mn}-\mathrm{O}$ bond which are characteristic for the parameters of the elongated octahedra in the parent $\mathrm{LaMnO_3}$. According to [22], in $\mathrm{La_{1-x}Sr_xMnO_3}$ the presence of such insulating inclusions is seen up to $x = 0.35$. The local neutron probe [22,53] can not resolve the size and the pattern of the distorted areas. One possible view may be to consider them as randomly positioned centers or the JT "polarons" with a scale $\sim 15-20$ Å. However, we have to keep in mind, that in the 3D percolative regime, the percolative paths (infinitely connected clusters) may coexist for both phases simultaneously. The analysis of low temperature metallic properties performed in the previous Section, seems to indicate that at least for concentrations $x \sim 0.3$, the ferromagnetic phase component, in the first approximation, occupies most of the bulk with other phase embedded into it and also seen as reasonably small scattering centers.

The Kirkpatrick relation (30) is expected to be approximately correct in homogeneous media regime, near T_{c}, where onset of ferromagnetism may be interpreted as the simultaneous onset of a new (metallic) mechanism for conductivity. As it was pointed out at the end of Section 6, equation (30) may be satisfied reasonably well. At the same time, it has been already known [46] that in $\mathrm{La_{0.8}Sr_{0.2}MnO_3}$ the peak temperature, T_{p}, and the Curie temperature, T_{c}, do not coincide ($T_{\mathrm{p}} =$ and $T_{\mathrm{c}} =$). These experiments were mostly considered in the literature as a crossover [6] in which conductivity regime *via* the thermal hopping of polarons localized by the thermal lattice disorder cedes sharply to a metallic regime with a short mean free path. In recent STM experiments [54] it has been successfully demonstrated that even around T_{c} the regime in $\mathrm{La_{0.7}Ca_{0.3}MnO_3}$ is better described as a coexistence of the two percolative phases: metallic and insulating ones. The characteristic scale for sizes of subphases having the shape of smooth clouds are from tens to hundreds of nanometers.

Another experimental support comes from the Mössbauer spectroscopy measurements [55]. The strong paramagnetic signal has been observed at $T > T_{\mathrm{c}}$. Decrease in T leads to the appearance at $T < T_{\mathrm{c}}$ of the strong signature of the ferromagnetic state, namely the "6 picks" structure in the Mössbauer signal. However, even at $T < T_{\mathrm{c}}$ the paramagnetic signal persists up to $T \simeq 20$ K, which is much lower then T_{c}. These studies strongly support the existence of the two phases and therefore the percolative scenario.

8 Conclusions

We have discussed above two major issues in doped manganites: 1. the concept of percolation, leading, as it was first predicted in [9], to the new understanding of the phenomena related to the phase separation, which takes place in these materials at low enough concentrations; 2. the possibility to interpret some low temperature data in the habitual band (or Fermi liquid) picture. The latter makes possible to suggest an unifying view which circumvent the often raised concerns regarding the role of strong interactions, importance of which is commonly expected in the transition metal oxides [17]. The Fermi liquid approach is a selfconsistent theory, which of course, may be broken at strong interactions. The only way to justify the Fermi liquid approach is to see whether the experimental results do fit the theory predictions or not. As it was shown above, the theory works reasonably well at $x = 0$ and at $x \sim 0.3$ for $\mathrm{La_{1-x}Sr_xMnO_3}$, probably because the DE-mechanism results in rather effective de-localization while the JT-effect partially takes care of the Coulomb interaction. In the intermediate regime with respect to x, the tendency towards the phase segregation turns out to have a percolative character and, therefore, theoretical analysis becomes much more complicated.

The question whether the samples quality is an intrinsic property or may be further improved, seems to be of principle importance. Experience with LSMO materials [45] implies that attempts made to improve the crystals quality are worth of trying. Already the LSMO samples with $1/\tau \sim 20$ K are encouraging, being reasonably close to the possibility of studying metallic manganites by methods traditional to the normal physics of metals, including the possibility of the de Haas-van Alphen studies in fields of the order of $30-40$ Teslas.

L.P.G. and V.Z.K. gratefully acknowledge H.D. Drew, T. Egami, J. Lynn, S. von Molnar for numerous stimulating discussions. The work was supported (L.P.G. and M.O.D.) by the National High Magnetic Field Laboratory through NSF Cooperative Agreement # DMR-9527035 and the State of Florida.

References

1. J.M.D. Coey, M. Viret, S. von Molnar, Adv. Phys. **48**, 167 (1999).
2. A.P. Ramirez, J. Phys. Cond. Matter **9**, 8171 (1997).
3. C. Zener, Phys. Rev. **81**, 440 (1951).
4. C. Zener, Phys. Rev. **82**, 403 (1951).
5. P.W. Anderson, H. Hasegawa, Phys. Rev. **100**, 675 (1955).
6. A.J. Millis, B.I. Shraiman, R. Mueller, Phys. Rev. Lett. **77**, 175 (1996).
7. A.J. Millis, R. Mueller, B. Shraiman, Phys. Rev. B **54**, 5389 (1996).
8. H. Roëder, Jun Zang, A.R. Bishop, Phys. Rev. Lett. **76**, 1356 (1996).
9. L.P. Gor'kov, V.Z. Kresin, JETP Lett. **67**, 985 (1998).
10. W. Pickett, S. Singh, Phys. Rev. B **53**, 1146 (1996).
11. J.H. Jung, K.H. Kim, T.W. Noh, E.J. Choi, Jaejun Yu, Phys. Rev. B **57**, R11043 (1998); Y. Okimoto, T. Katsufuji, T. Ishikawa, A. Urushibara, T. Arima, Y. Tokura, Phys. Rev. Lett. **75**, 109 (1995) and references therein.

12. J. Kanamori, J. Appl. Phys. (Suppl.) **31**, 145 (1961).
13. K. Kugel, D.I. Khomskii, Sov. Phys. - Usp. **25**, 231 (1982).
14. L.P. Gor'kov, Soviet Phys. - Uspekhi **41**, 589 (1998).
15. D.I. Khomskii, G.A. Sawatzky, Solid State Comm. **102**, 87 (1997).
16. M.D. Kaplan, B.G. Vekhter, *Cooperative Phenomena in Jahn-Teller Crystals* (Plenum Press, N.Y. - London, 1995).
17. J.B. Goodenough, *Magnetism and the Chemical Bond* (N.Y. - London, 1963).
18. P.W. Anderson, Phys. Rev. **115**, 2 (1959).
19. S.E. Lofland, S.M. Bhagat, K. Ghosh, R.L. Green, S.G. Karabashev. D.A. Shulyatev, A.A. Arsenov, Y. Mukovskii, Phys. Rev. B **56**, 13705 (1997).
20. M.O. Dzero, L.P. Gor'kov, V.Z. Kresin, Solid State Comm. **112**, 707 (1999).
21. J. van den Brink, D. Khomskii, Phys. Rev. Lett. **82**, 1016 (1999).
22. D. Louca, T. Egami, Phys. Rev. B **59**, 6193 (1999); J. Supercond. **12**, 23 (1999).
23. K. Ghosh (private communication).
24. T. Okuda, A. Asamitsu, Y. Tomioka, T. Kimura, Y. Taguchi, Y. Tokura, Phys. Rev. Lett. **81**, 3203 (1998) and referencies therein.
25. Y. Okimoto, T. Katsufuji, T. Ishikawa, T. Arima, Y. Tokura, Phys. Rev. B **55**, 4206 (1997).
26. B. Shklovskii, A. Efros, *Electronic properties of Doped Semiconductors* (Springer-Verlag, Berlin 1984).
27. H. Scher, R. Zallen, J. Chem. Phys. **53**, 3759 (1970); for review see G. Deutcher, in *Chance and Matter*, edited by J. Souletie, J. Vannimenus, R. Stora (Elsevier Amsterdam, 1987), p. 1.
28. A. Urushibara, Y. Moritomo, T. Arima, A. Asamitsu, G. Kido, Y. Tokura, Phys. Rev. B **51**, 14103 (1995).
29. Y. Tokura, A. Urushibara, Y. Moritomo, T. Arima, A. Asamitsu, G. Kido, N. Furukawa, J. Phys. Soc. Jpn. **63**, 3931 (1994).
30. N. Furukawa, J. Phys. Soc. Jpn. **65**, 1174 (1996).
31. E.M. Lifshitz, L.P. Pitaevskii, *Statistical Physics, Part 2* (Pergamon Press, Oxford 1989), p. 227.
32. A. Takahashi, H. Shiba, Eur. Phys. J. B **5**, 413 (1998).
33. S.-W. Cheong, H.Y. Hwang, C.H. Chen, B. Batlogg, L.W. Rupp Jr., S.A. Carter, Phys. Rev. B. **49**, 7088 (1994).
34. Y. Tomioka, A. Asamitsu, Y. Moritomo, H. Kuwahara, Y. Tokura, Phys. Rev. Lett. **74**, 5108 (1995).
35. H. Kawano, R. Kajimoto, H. Yoshizawa, Y. Tomioka, H. Kuwahara, Y. Tokura, Phys. Rev. Lett. **78**, 4253 (1997).
36. T. Akimoto, Y. Maruyama, Y. Maritomo, A. Nakamura, Phys. Rev. B **55**, R5594 (1998).
37. R. Mahendiran, M.R. Ibarra, A. Maignan, F. Millange, A. Arulraj, R. Mahesh, B. Raveau, C.N.R. Rao, Phys. Rev. Lett. **82**, 2191 (1999).
38. Y. Tokura, H. Kuwahara, Y. Moritomo, Y. Tomioka, A. Asamitsu, Phys. Rev. Lett. **76**, 3184 (1996).
39. M. Tokunaga, N. Miura, Y. Tomioka, Y. Tokura, Phys. Rev. B **57**, 5259 (1998).
40. H. Kuwahara, T. Okuda, Y. Tomioka, A. Asamitsu, Y. Tokura, Phys. Rev. Lett. **82**, 4316 (1999); Science **270**, 961 (1995).
41. M. Tokunaga, N. Miura, Y. Tomioka, Y. Tokura, Phys. Rev. B **57**, 5259 (1998).
42. J.A. Fernandez-Baca, P. Dai, H.Y. Hwang, C. Kloc, S.-W. Cheong, Phys. Rev. Lett. **80**, 4012 (1998).
43. A.H. Moudden, L. Vasiliu-Doloc, L. Pinsard, A. Revcolevschi, Physica B **241-243**, 276 (1998).
44. Y. Endoh, K. Hirota, J. Phys. Soc. Jpn. **66**, 2264 (1997).
45. M. Quijada, J. Cerne, J.R. Simpson, H.D. Drew, K.H. Ahn, A.J. Millis, R. Shreekala, R. Ramesh, M. Rajeswari, T. Venkatesan, Phys. Rev. B **58**, 16093 (1998).
46. S.E. Lofland, S.M. Bhagat, H. Ju, G. Xiong, T. Venkatesan, R. Green, J. Appl. Phys. **79**, 5166 (1996).
47. V. Gantmakher, Y. Levinson, *Carrier Scattering in Metals and Semiconductors* (North-Holland, Amsterdam, 1987), p. 139.
48. G. Mahan, *Many Particle Physics* (Plenum Press, New-York, 1993), p. 686.
49. A.V. Boris, N.N. Kovaleva, A.V. Bazhenov, P.J.M. van Bentum, Th. Rasing, S.-W. Cheong, A.V. Samoilov, N.-C. Yeh, Phys. Rev. B **59**, R697 (1999).
50. T.G. Perring, G. Aeppli, S.M. Hayden, S.A. Carter, J.P. Remeika, S.-W. Cheong, Phys. Rev. Lett. **77**, 711 (1996).
51. H.Y. Hwang, P. Dai, S.-W. Cheong, G. Aeppli, D.A. Tennant, H.A. Mook, Phys. Rev. Lett. **80**, 1316 (1998).
52. P.-G. de Gennes, Phys. Rev. **118**, 141 (1960).
53. S.J.L. Billinge, T. Egami, Phys. Rev. B **47**, 14386 (1993).
54. M. Fäth, S. Freisem, A.A. Menovsky, Y. Tomioka, J. Aarts, J.A. Mydosh, Science **285**, 1540, (1999).
55. V. Chethetsky, A. Nath, H. Jeu, R. Green, Low. Temp. Phys. **23**, 545 (1997).